

# The Spatial Orientation of Planetary Nebulae Within the Milky Way

Walter Weidmann<sup>1,2</sup> & Rubén J. Díaz<sup>1</sup>

Received \_\_\_\_\_; accepted \_\_\_\_\_

arXiv:astro-ph/0505092v1 5 May 2005

---

<sup>1</sup>Observatorio Astronómico de Córdoba, UNC, Laprida 854, 5000 Córdoba, Argentina;  
walter@mail.oac.uncor.edu, diaz@mail.oac.uncor.edu

<sup>2</sup>SeCyt, Universidad Nacional de Córdoba, Argentina

## ABSTRACT

We investigate the spatial orientation of a homogenous sample of elongated Planetary Nebulae (PN) in order to determine the orientation of their apparent major axis respect to the Milky Way plane. We present some important geometrical considerations that may have been overlooked by the previous works on the subject. We find that there are some regions on the sky (for example the galactic center), where some correlation could exist between the orientation of the major axis of some PNe and the Galactic equator. The distribution of positions angles (PA) is quantitatively different from a random orientation of the planetaries in the Galaxy. There appear to be no clear mechanisms whereby this non-random distribution may be explained. Considering the present knowledge of PN and stellar evolution, we suggest that “extrinsic” phenomena should provide an important influence in the morphology of such nebulae.

*Subject headings:* methods: statistical – stars: AGB and post-AGB – ISM: evolution  
– (ISM:) planetary nebulae: general – Galaxy: general

## 1. INTRODUCTION

Since Charles Messier registered the first Planetary Nebulae (Dumbbell Nebula in Vulpecula) on July 12, 1764 until the present time, over one thousand of these beautiful objects were found in our Galaxy and much more in nearby galaxies. It is well known that PN have different shapes but, in most cases, the projection of a nebula onto the sky has a defined extension axis.

However, the study of the orientation of many kind of phenomena such as supernova remnants (Gaensler 1998), orbits of binary systems (Brazhnikova et al. 1975), rotation of individual stars (Hensberge et al. 1979), has been of broad astrophysical interest. This sort of study provides information about formation, evolution and death of the stars.

The orientation of the projected major axis of the PNe was rarely studied and the results that were found are still contradictory.

Shain (1956) and Gurzadyan (1958) made the pioneer works about the orientation of PN. They worked with very small samples from the Curtis catalogue (1917) and their conclusions were contradictory. Shain found that the angle between the semi-major axis of PNe and the galactic equator was small for objects with low latitudes. On the other hand Gurzadyan did not found any correlation and used this to deduce that the magnetic field could not influence the shape of PN. At the present time both papers only have a historical character.

The first works to determine spatial orientations of PN with a significant number of objects were those of Grinin & Zvereva (1968), and Melnick & Harwitt (1974). These works are more critical than early ones and both papers conclude that PNe are aligned with the plane. The hypothesis suggested as explanations of these non-random orientations were based in the effect of the ambient magnetic field and interactions with interstellar medium.

The works of Phillips (1997) and Corradi, Aznar & Mampaso (1998; hereafter CAM98) are the most recent papers about global PN orientation. In both cases, the images examined had high quality and the determination of PA have small errors, but they did not study the orientation of PN over a specific region of the sky. The sample of Phillips was culled from a variety of published images complemented with broad band survey plates, whereas the sample of Corradi and coworkers come mainly from three different narrow band surveys.

In this paper we take up again the investigations of the orientation of elongated PN with respect to the Milky Way plane and make a careful search of sky regions where the PNe orientations appear to have certain correlations with the Galactic plane direction. The sample was extracted from a unique catalogue in such a way that it was homogenous. The number of PNe included in this work is 355. In the selection of objects we do not consider its detailed morphology. The analysis is performed through Sections 3 to 5, the results are presented and discussed in Sections 6 and 7.

## 2. SELECTION OF THE SAMPLE

The sample was extracted from the Catalogue of Galactic Planetary Nebulae updated version 2000 (L. Kohoutek 2001), hereafter CGPN2000. This extensive list includes 1510 true PNe. The selection criteria employed to obtain our final sample were:

1. Angular size larger than  $10''$ .
2. Objects clearly visible in the DSS plates (surface brightness  $< 17$  mag/arcmin<sup>2</sup>).
3. Elongated shape.

In order to assure the homogeneity of the sample after the third criterium, the selection was made only by inspecting the images from the DSS survey plate in the red band. This

band includes the main red nebular lines  $H\alpha$  (6563 Å), [NII]  $\lambda\lambda$  6548 Å 6584 Å, [SII]  $\lambda\lambda$  6717 Å 6731 Å.

After a careful examination of more than 500 PNe in the initial list (obtained after criterium 1), we arrived to the final sample that contains 189 PNe distributed in four regions. The remaining objects were planetaries with apparent circular shape, low surface brightness or very peculiar morphology.

### 3. MEASUREMENT OF POSITION ANGLES

The position angles (PA), of the projected major axis over the sky, were measured for all the PNe included in the final sample. PA are measured following the usual convention: from the north towards the east. These angles are measured within the equatorial coordinates system so we call it EPA.

The directions of the elongated axis were estimated visually by fixing the line that better represents the long symmetry axis of the PN. The angle that this line forms with the north was the EPA. For bipolar structures the EPA was measured with respect to the direction of the outflow of the objects. The uncertainties of EPA are estimated following the criterium of CAM98: all measurements were repeated independently by two of us. The largest difference between both measurements was 8°. The measuring criteria are exemplified in Fig. 1.

In spite of the fact that all previous works determined the EPA visually we tried to obtain those angles through different software approaches, but the problem was that this sort of software is still not powerful enough to extract information from noisy objects. PN are usually located in highly populated Milky Way fields and in many cases do not show structure complete at the same surface brightness. This patchy structure and the star

images make the software approach still difficult.

An example of a more refined criterion of EPA measurement, constitutes an attentive comparison between the figures 1c and 1d. In spite of the fact that both objects present the characteristic belt of bipolar planetary nebulae, in the case of NGC 5189 the structures that appear in both sides of the apparent belt have not hemispherical appearance as the case shown in figure 1d. The orientation that is marked in the figure takes into account that the brilliant knot at the E of the main body external part, is of appearance totally nebular when the original image is inspected. Considering that the criterion of determination is based mainly on the external morphology, the major axis of the PN is well determined. This complex case represents a limit case where the assigned EPA could differ among researching with varying criteria.

On the other hand the values of EPA that we obtain are, in general, comparable with the values obtained in the work of CAM98 for objects present in both samples. A detailed comparison is described in section 7.

#### 4. TRANSFORMATION TO THE GALACTIC SYSTEM

The EPA are measured relative to the equatorial coordinates system, in order to transform this position angle to the galactic system we need to compute the angle  $\beta$  which is subtended at the position of each object by the direction of the equatorial north and the galactic north.

$$\beta = \frac{\cos \delta_0 \sin(\alpha_0 - \alpha)}{\cos b}$$

Where  $\delta_0$  and  $\alpha_0$  are the equatorial coordinates of the galactic North Pole.  $\alpha$  and  $b$  are the equatorial right ascension and galactic latitude coordinates respectively (both

coordinates were extracted from CGPN2000). Then the galactic position angle (GPA) is defined as the position angle of the major axis of the apparent nebular elongation, measured from the direction of the galactic north towards the east (Table 5).

$$GPA = EPA - \beta$$

It should be noted here that the EPA are computed in the interval  $[0^\circ, 180^\circ]$  in the same way as, e.g., Phillips (1997). The values are reported and used here in the same range, but some authors (e.g. CAM98) report them to the interval  $[0^\circ, 90^\circ]$  assuming a priori a symmetric problem, in the sense that a preferred orientation of the PNe elongations very nearly to the galactic equator will be easier to detect. The problem with this treatment of the EPA is that it would blur any other preferred orientation that is not very near to the galactic equator (Fig. 2).

## 5. STUDIED REGIONS

The orientations for individual planetary nebulae is presented in Table 5, which is also available on request to the authors. In order to avoid information degradation by projection effects, we did not include in our study objects with  $|b| > 20^\circ$ . Nevertheless, the number of objects far from the galactic plane is not statistically significant. To study the orientation of the sample, we selected four angular sectors: those defined by the galactic center and anti-center, and the perpendicular directions (Table 1).

The regions were defined in angular range in such a way that there was enough number of objects to do a statistical analysis. But they should not be so large in angular extent that any absolute orientation respect to the galactic system would be deleted by the superposition of different projections to the observer. It must be taken into account, that the projection effects over the observer would delete the evidence of some preferred

orientations if the data are compiled and analyzed as a whole set without any regard to the position respect to the observer and the galactic center. All the previous works have treated the data as a whole set, and we think that in this way important information could have been overlooked.

## 6. RESULTS

The region that shows a distribution of GPA with marked non-random characteristics is the region with center towards the galactic center. In the other regions, the low number of objects precludes detection of any clear trend. The distribution of GPA of these regions are presented in Fig. 3.

If the distribution of the  $\mathbf{N}$  objects of the sample in each sector were random, with the same probability of finding an elongated object with its axis towards any PA, when  $\mathbf{j}$  angular boxes are defined in the range  $[0^\circ, 180^\circ]$ , it could be expected an average population of  $\mathbf{N}/\mathbf{j}$  objects per bin. The frequency of all the possible values would be an angular positions distribution, with a dispersion  $\sigma = (\mathbf{N}/\mathbf{j})^{1/2}$ . In Table 2 we show the expected average and dispersion for each region, and the number of peaks observed above  $2\sigma$  and  $1\sigma$ .

The calculated barycenters for each peak, determined within a window of  $60^\circ$ , are summarized in Table 3. A thorough test can be preformed by applying a simple binomial test, as proposed by Siegel (1956) and applied by Hutsemékers (1998). It gives the probability  $P_s$  that a random distribution has  $L_s$  angles (of a set of  $N$  objects) in the interval  $[P_m - \alpha, P_m + \alpha]$ . In our case  $P_m$  is the peak barycenter. Such probability is defined as:

$$P_s = \sum_{l=L_s}^N \left(\frac{\alpha}{90}\right)^l \left(1 - \frac{\alpha}{90}\right)^{N-l} \binom{N}{l}$$

Table 4 shows the probability of randomness for each observed peak using  $\alpha = 20^\circ$  and  $\alpha = 10^\circ$  (note that when  $\alpha = 20^\circ$  the probability that the right peak of region I is random, is only  $P = 0.016$ ). In region I, the distribution has two peaks with a separation of  $\sim 80^\circ$  (or  $\sim 100^\circ$  in the opposite sense) in the directions defined by the peaks.

Following the clue provided by some similarity of the result in regions III and IV, we added the distributions found for regions I and II (Fig. 4a) and for regions III and IV (Fig. 4b).

The two distributions in Fig. 4b show one peak over  $2\sigma$  and 1 peak over  $1\sigma$ , in both cases with a peak separation of  $80^\circ$ . Here the separation is considered as the minimum angular distance between both peaks. Moreover as both distributions are in opposite sides of the sky, is natural to measure the separation in opposite sense.

It should be noted that the position angles are being measured with the NESW convention, without any regard to the absolute orientation of the objects respect to the observer. Then if some absolute orientation would be common to most of the objects and considering that the observer is in the center of the sky band over which the objects appear projected, the sense of measuring of the position angles in opposite regions (e.g. I and II) should be inverted by making **180 - GPA** in the opposite regions.

Amazingly, the transformation of the data in regions III+IV (Fig. 4b) gives a distribution resembling that of regions I+II: a major peak and a secondary one  $80^\circ$  before.

We also carried out the Kolmogorov-Smirnov (K-S) test to have an alternative evaluation of the randomness of the observed distribution. This requires the calculation of  $D_{max}$ : the absolute value of the maximum deviation between the observed ( $S_N(x)$  with  $N_1$  points) and theoretical ( $P(x)$  with  $N_2$  points) cumulative distribution function (Press et al. 1992). The significance can be written as the following sum:

$$Q_{ks} = 2 \sum_{j=1}^{\infty} (-1)^{(j-1)} e^{-2j^2\lambda^2}$$

Where  $\lambda = (\sqrt{N_e} + 0.12 + 0.11/\sqrt{N_e})D_{max}$  and  $N_e = N_1N_2/(N_1 + N_2)$  that is the effective number of data points of the samples.

This test gave us a probability, that our data follow a random distribution, of 82% for region I, 68% for region II, 97% for region III and 35% for region IV.

As an alternative we tried to perform a variation of K-S test: the Kuiper (K-P) test which is more sensible than K-S test in some kind of circular distributions.

To perform this test we have to calculate  $V = D_+ + D_-$ , which is the sum of the maximum distance of  $S_N(x)$  above and below  $P(x)$ . A good approximation for the significance is:

$$Q_{kp} = 2 \sum_{j=1}^{\infty} (4j^2\lambda^2 - 1)e^{-2j^2\lambda^2}$$

Where  $\lambda = (\sqrt{N_e} + 0.155 + 0.24/\sqrt{N_e})V$

The result that we obtained with K-P test for our region I (with the strongest signal) is  $Q_{KP} = 67\%$ , which seems to be not a convincing one. This result lead us to think that these tests could not be fully applicable to our kind of data. Caution should be taken when applying all varieties of K-S test, because they lack the ability to discriminate some kind of distributions. For example, consider a probability distribution with a narrow notch within which the probability falls to zero. Such a distribution is of course ruled out by the existence of even one data point within the notch, but, because of its cumulative nature, K-S test would require many data points in the notch before signaling a discrepancy (Press et al. 1992).

To probe this kind of behavior, we generated a random distribution of 72 GPA and after that we added 10 GPA values distributed in the first bin (Fig. 6). This distribution has a average of 9.1 GPA per bin and a dispersion of  $\sigma = 3.0$ . In this way, the first bin shows a signal over  $3\sigma$ . Now if we apply both tests to this artificial sample we obtain the next probabilities, that this data follow a random distribution:  $Q_{KS} = 17\%$  and  $Q_{KP} = 67\%$  (Fig. 7). We have verified that there is no way to generate 67 cases and not even 17 cases of a  $3\sigma$  peak in 100 fully random samples.

Therefore we conclude that although K-S and K-P tests are well suited to analyze non random global trends in samples, they are strongly insensitive to the presence of a local non-random feature.

## 7. DISCUSSION

We studied the orientation of all PNe of our sample (without separating it in regions) and we do not see a clear preferential orientation of long axis of PN respect to the galactic plane. This distribution of GPA is similar to that observed by CAM98. We tried to double check our results by applying our analysis to the data published by CAM98, performing a suitable analysis to take over the ambiguity of the position angles (assigned to the range  $[0^\circ, 90^\circ]$ ).

More precisely, the sample of CAM98 includes 208 objects (counting the object M2-55 in only one list); 69 of them are in both samples (the object that CAM98 put in the list of ellipticals as PC 4, is in fact PB 4); 85 are outside our four regions; 50 were not measured because they are too small; have strange morphology or circular appearance; and 4 objects are not true PN (Bl Cru, CRL 2688, M 1-91, M 1-92).

75% of the 69 objects that are in both samples, have his GPA in good agreement

( $\pm 10^\circ$ ) with our measurement. Moreover, the distribution of GPA from those objects from CAM98 whose coordinates are in region I, shows a clear peak over  $3\sigma$  (Fig. 5, 48 objects), whose barycenter is in  $100^\circ \pm 15^\circ$ , a position similar, within the uncertainties, to one of the peaks in our Fig. 3.

The differences could be mainly caused by the fact that they employed deep narrow-band images. It could be expected that the geometrical properties of the objects change as distinct ionization layers are imaged through different filters, more precisely, we think that the left peak (e.g. We 1-4) in our broad band study could be arose in the measuring of the PN equatorial belt apparent axis instead of the faint external envelope. This should not occur in the deep narrow band images of the CAM98 sample, and could explain the absence of the second peak in that sample.

In order to probe if this distribution of GPA found in the four regions has a distance modulation we considered objects statistically far and close. To do it, we separated objects in each region by its angular size (objects with great angular size were considered closer than the ones with small angular size). The results that we obtained in the four regions show that the distribution of GPA for larger PNe has the same shape than the smaller PNe. So there is not evidence about a distance effect.

In the same sense we tried to relate the PA of the long axis of PN with respect to the Gould Belt, the plane defined by nearby stars of young population, mainly O and B stars (Cameron et al. 1994). The result found shows a noisy distribution of PA.

Several studies have related bipolar PNe with binary progenitors (Bond et al. 1990). The antecedents about the orientations of the orbits of binary stars do not provide any comparable result. Notwithstanding it must be remarked that a thorough analysis should be made, keeping in mind the new geometric considerations carried out in this work.

## 8. FINAL REMARKS

The data on PA of planetary nebulae show that preferred orientations seem to exist. This preferred orientations are clearer in the zones near to the galactic center, and the distribution of galactic position angles could have peaks not exactly aligned with the Milky Way plane. The PNe towards the galactic center have an orientation distribution with a peak near to the galactic plane ( $GPA \simeq 120^\circ$ ), with a randomness probability as small as 0.016.

Besides the conclusions hold by the results, we presented here some important geometrical and analytical considerations that have been possibly overlooked by the previous works on the subject.

There is also some suggestion in the data of some absolute preferred orientations in the Galaxy. The possible implications are of broad astrophysical interest and we hope that they stimulate more detailed studies.

This work was partially supported by Agencia Cordoba Ciencia and CONICET of Argentina. We wish to thank the referee for valuable and constructive comments.

## REFERENCES

- Acker, A., Ochsenbein, F., Stenholm, B., Tylanda, R., Marcout, J., Schohn, C. 1992, Strasbourg-ESO catalogue of Planetary Nebulae. ESO, Garching.
- Bond, H. E., Livio, M. 1990, *ApJ*, 335, 568
- Brazhnikova, E.F., Dagaev, M.M. & Radzievskii, V.V. 1975, *AZh*, 52, 546
- Corradi, R., Aznar, R. & Mampaso, A. 1998, *MNRAS*, 297, 617
- Gaensler, B.M. 1998, *ApJ*, 493, 781
- Grinin, V.P. & Zvereva, A.M. 1968, *Astrofizika*, 4, 135
- Gurzadyan, G.A. 1969, *Planetary Nebulae*; eds. Gordon & Breach
- Hensberge, H., van Rensbergen, W., Deridder, G. & Goossens, M. 1979, *A&A*, 75, 83
- Hutsemékers, D. 1998, *A&A*, 332, 410
- Kohoutek, L., *Catalogue of galactic planetary nebulae*, Updated version 2000, Hamburg: Hamburger Sternwarte, 2001 294 p. *Abhandlungen aus der Hamburger Sternwarte* 12
- Melnick, G. & Harwit, M. 1974, *MNRAS*, 171, 441
- Phillips, J.P. 199, *A&A*, 325, 755
- Press, W. H., Teukolsky, S.A., Vetterling, W.T. & Flannery, B.P. 1992. *Numerical Recipes in Fortran*, Second Edition; eds. Cambridge University Press
- Siegel, S. 1967. *Nonparametric Statistics*; eds. McGraw-Hill

Table 1. Sampled galactic sectors

Sector	l range [°]	b range [°]	Number of objects
Galactic center (region I)	-30 a 30	-20 a 20	78
Local motion apex (region II)	60 a 120	-20 a 20	47
Galactic anti-center (region III)	150 a 210	-20 a 20	19
Local motion antapex (region IV)	240 a 300	-20 a 20	45

Table 2. Distribution peaks observed in Fig. 3

Regions	Number of objects	Average	Dispersion	$2\sigma$ peaks	$1\sigma$ peaks
I	78	8.7	2.9	1	1
II	47	5.2	2.3	-	2
III	19	2.1	1.5	-	1
IV	45	5.0	2.2	-	1

Table 3. Barycenters of the peaks observed in Fig. 3

Regions	Barycenter 1[°]	Barycenter 2[°]	Separation [°]
I	$22 \pm 14$	$119 \pm 16$	83
II	$2 \pm 12$	$61 \pm 15$	59
III	-	$161 \pm 16$	-
IV	$83 \pm 16$	-	-

Table 4. Randomness probabilities of each sector with a peak width of  $20^\circ$  ( $\alpha = 10^\circ$ ) and  $40^\circ$  ( $\alpha = 20^\circ$ )

Regions	(Left peak) <sub>20</sub>	(Right peak) <sub>20</sub>	(Left peak) <sub>10</sub>	(Right peak) <sub>10</sub>
I	0.367	0.016	0.011	0.089
II	0.231	0.345	0.071	0.071
III	-	0.419	-	0.052
IV	0.058	-	0.057	-

Table 5. Data

Name	l [°]	b [°]	EPA [°]	GPA [°]
IC 4634	0.3	12.2	153	27
K1-4	1.0	1.9	155	33
NGC 6369	2.4	5.9	167	44
IC 4673	3.5	-2.4	126	7
M 1-28	6.0	3.1	14	73
M 2-34	7.8	-3.7	177	59
NGC 6445	8.0	3.9	51	110
A 41	9.6	10.5	143	21
NGC 6309	9.6	14.8	56	114
NGC 6537	10.1	0.7	38	99
M 2-9	10.8	18.1	179	57
DeHt 10	11.4	17.9	175	53
We 4-5	13.7	-15.3	141	27
SaWe 3	13.8	-2.8	133	15
A 44	15.6	-3.0	131	13
M 1-54	16.0	-4.3	104	167
DeHt 3	19.4	-13.6	8	73
M 3-28	21.8	-0.5	2	64
MaC 1-13	22.5	1.0	26	88
M 4-9	24.2	5.9	168	50
A 60	25.0	-11.7	103	166

Table 5—Continued

Name	l [°]	b [°]	EPA [°]	GPA [°]
DeHt 2	27.6	16.9	44	107
WeSb 3	28.0	10.3	149	31
A 48	29.0	0.5	37	99
NGC 6751	29.2	-5.9	81	144
NGC 6853	60.8	-3.7	129	6
He 2-437	61.3	3.6	77	138
NGC 6905	61.4	-9.6	161	36
M 2-48	62.4	-0.3	67	125
NGC 6720	63.1	14.0	57	123
We 1-9	65.1	-3.5	70	126
He 1-6	65.2	-5.7	122	177
M 1-75	68.8	0.0	152	28
K 3-46	69.2	3.8	110	168
NGC 6894	69.4	-2.6	145	20
K 3-58	69.6	-3.9	83	137
A 74	72.7	-17.1	52	99
GM 1-11	73.0	-2.2	65	119
Anon	75.6	4.3	109	166
A 69	76.3	1.2	54	108
DD 1	78.6	5.2	81	137
M 4-17	79.6	5.8	118	174

Table 5—Continued

Name	l [°]	b [°]	EPA [°]	GPA [°]
A 78	81.2	-14.9	146	9
K 4-55	84.2	1.0	85	135
A 71	84.9	4.4	15	68
We 2-245	87.4	-3.8	137	1
NGC 7048	88.7	-1.6	15	60
NGC 7026	89.0	0.3	4	51
Sh 1-89	89.8	-0.6	50	95
We 1-11	91.6	1.8	49	95
K 3-79	92.1	5.8	132	1
M 1-79	93.3	-2.4	88	129
NGC 7008	93.4	5.4	38	86
A 73	95.2	7.8	38	87
A 75	101.8	8.7	94	137
A 80	102.8	-5.0	19	48
A 79	102.9	-2.3	20	51
M 2-51	103.2	0.6	151	4
M 2-52	103.7	0.4	116	148
KLW 8	104.1	-1.4	40	70
NGC 7139	104.1	7.9	47	86
M 2-53	104.4	-1.6	95	124
NGC 7354	107.8	2.3	17	45

Table 5—Continued

Name	l [°]	b [°]	EPA [°]	GPA [°]
K 1-20	110.6	-12.9	154	169
K 3-88	112.5	3.7	45	66
A 84	112.9	-10.2	172	6
A 83	113.6	-6.9	34	47
A 82	114.0	-4.6	46	59
We 2-262	116.0	0.1	172	4
M 2-55	116.2	8.5	38	55
A 86	118.7	8.2	115	125
BV 5-1	119.3	0.3	53	59
IC 2149	166.1	10.4	73	11
CRL 618	166.4	-6.5	99	49
Pu 2	173.5	3.2	47	169
H 3-29	174.2	-14.6	158	107
Pu 1	181.5	0.9	50	170
WeSb 2	183.8	5.5	33	152
NGC 2371	189.1	19.8	129	61
M 1-7	189.8	7.8	153	90
J 320	190.3	-17.8	174	117
HaWe 8	192.5	7.2	134	71
J 900	194.2	2.6	83	21
NGC 2022	196.6	-11.0	32	152

Table 5—Continued

Name	l [°]	b [°]	EPA [°]	GPA [°]
A 14	197.8	-3.4	175	114
A 12	198.6	-6.3	15	134
A 19	200.7	8.4	65	2
We 1-4	201.9	-4.7	104	42
A 13	204.0	-8.5	47	165
K 3-72	204.8	-3.6	139	77
A 21	205.1	14.2	136	72
M 3-2	240.3	-7.6	42	160
M 3-4	241.0	2.3	141	83
M 3-1	242.6	-11.6	143	78
NGC 2452	243.3	-1.1	116	57
A 29	244.5	12.5	133	80
A 26	250.3	0.1	141	85
K 1-21	251.1	-1.6	160	103
K 1-1	252.6	4.4	36	163
K 1-2	253.5	10.7	101	52
VBRC 1	257.5	0.6	118	65
He 2-11	259.1	0.9	137	86
He 2-15	261.6	3.0	33	164
NGC 2818	261.9	8.5	90	45
He 2-7	264.1	-8.1	161	105

Table 5—Continued

Name	l [°]	b [°]	EPA [°]	GPA [°]
Wray 17-20	264.4	-3.6	22	150
NGC 2792	265.7	4.1	146	100
NGC 3132	272.1	12.3	167	131
He 2-18	273.2	-3.7	75	29
Lo 4	274.3	9.1	46	11
He 2-37	274.6	3.5	119	80
PB 4	275.0	-4.1	35	170
He 2-29	275.8	-2.9	55	12
Wray 17-31	277.7	-3.5	90	48
He 2-32	278.5	-4.5	159	117
VBRC 3	279.0	-3.2	56	16
He 2-36	279.6	-3.1	144	105
He 2-48	282.9	3.8	129	99
Hf 4	283.9	-1.8	13	160
ESO 215-04	283.9	9.7	143	118
IC 2448	285.7	-14.9	137	88
Wray 17-40	286.2	-6.9	102	67
Hf 38	288.4	0.3	94	69
Hf 39	288.9	-0.8	43	18
He 2-57	289.6	-1.6	119	95
Hf 48	290.1	-0.4	136	113

Table 5—Continued

Name	l [°]	b [°]	EPA [°]	GPA [°]
Wray 16-93	292.7	1.9	134	117
He 2-70	293.6	1.2	137	121
Lo 6	294.1	14.4	150	140
NGC 3918	294.6	4.7	138	126
He 2-72	294.9	-0.6	101	87
He 2-76	298.2	-1.7	83	75
NGC 4071	298.3	-4.8	43	34
K 1-23	299.0	18.4	3	179
HaTr 1	299.4	-4.1	131	124
He 2-82	299.5	2.4	162	157
Lo 9	330.2	5.9	82	120
He 2-153	330.6	-2.1	41	86
He 2-159	330.6	-3.6	173	39
Wray 16-189	330.9	4.3	72	112
He 2-145	331.4	0.5	113	156
He 2-161	331.5	-2.7	48	94
He 2-165	331.5	-3.9	36	83
Mz 3	331.7	-1.0	10	55
He 2-164	332.0	-3.3	82	129
HaTr 6	332.8	-16.4	55	119
He 2-152	333.4	1.1	150	14

Table 5—Continued

Name	l [°]	b [°]	EPA [°]	GPA [°]
HaTr 3	333.4	-4.0	157	26
MeWe 1-6	334.3	-1.4	125	172
IC 4642	334.3	-9.3	143	18
HaTr 4	335.2	-3.6	94	144
ESO 330-02	335.4	9.2	4	45
He 2-169	335.4	-1.1	3	51
DS 2	335.5	12.4	115	154
K 2-17	336.8	-7.2	139	13
NGC 6326	338.1	-8.3	54	110
He 2-155	338.8	5.6	61	106
Sa 1-6	340.4	-14.1	42	106
Lo 11	340.8	12.3	61	104
Lo 12	340.8	10.8	86	130
NGC 6026	341.6	13.7	63	106
NGC 6072	342.1	10.8	71	116
Sp 3	342.5	-14.3	144	28
H 1-3	342.7	0.7	146	17
He 2-207	342.9	-4.9	56	112
Pe 1-8	342.9	-2.0	61	114
SuWt 3	343.6	3.7	77	127
H 1-6	344.2	-1.2	145	18

Table 5—Continued

Name	l [°]	b [°]	EPA [°]	GPA [°]
MeWe 1-11	345.3	-10.2	41	102
IC 4637	345.4	0.1	0	53
He 2-175	345.6	6.7	94	143
Vd 1-6	345.9	3.0	110	162
IC 4663	346.2	-8.2	86	146
A 38	346.9	12.4	83	130
NGC 6337	349.3	-1.1	139	15
NGC 6302	349.5	1.1	83	137
H 1-26	350.1	-3.9	88	146
K 2-16	352.9	11.4	141	11
Wray 16-411	353.7	-12.8	87	152
M 3-14	355.4	-2.4	164	43
Th 3-3	356.5	5.1	102	157
M 2-24	356.9	-5.8	62	123
TrBr 4	357.6	1.0	26	84
Bl D	358.2	-1.1	149	28
M 3-39	358.5	5.4	35	91
NGC 6563	358.5	-7.3	60	121
M 3-9	359.0	5.1	116	173
A 40	359.1	15.1	72	125
Hb 5	359.3	-0.9	76	135

Table 5—Continued

---

---

Name	l [°]	b [°]	EPA [°]	GPA [°]
------	-------	-------	---------	---------

---

---

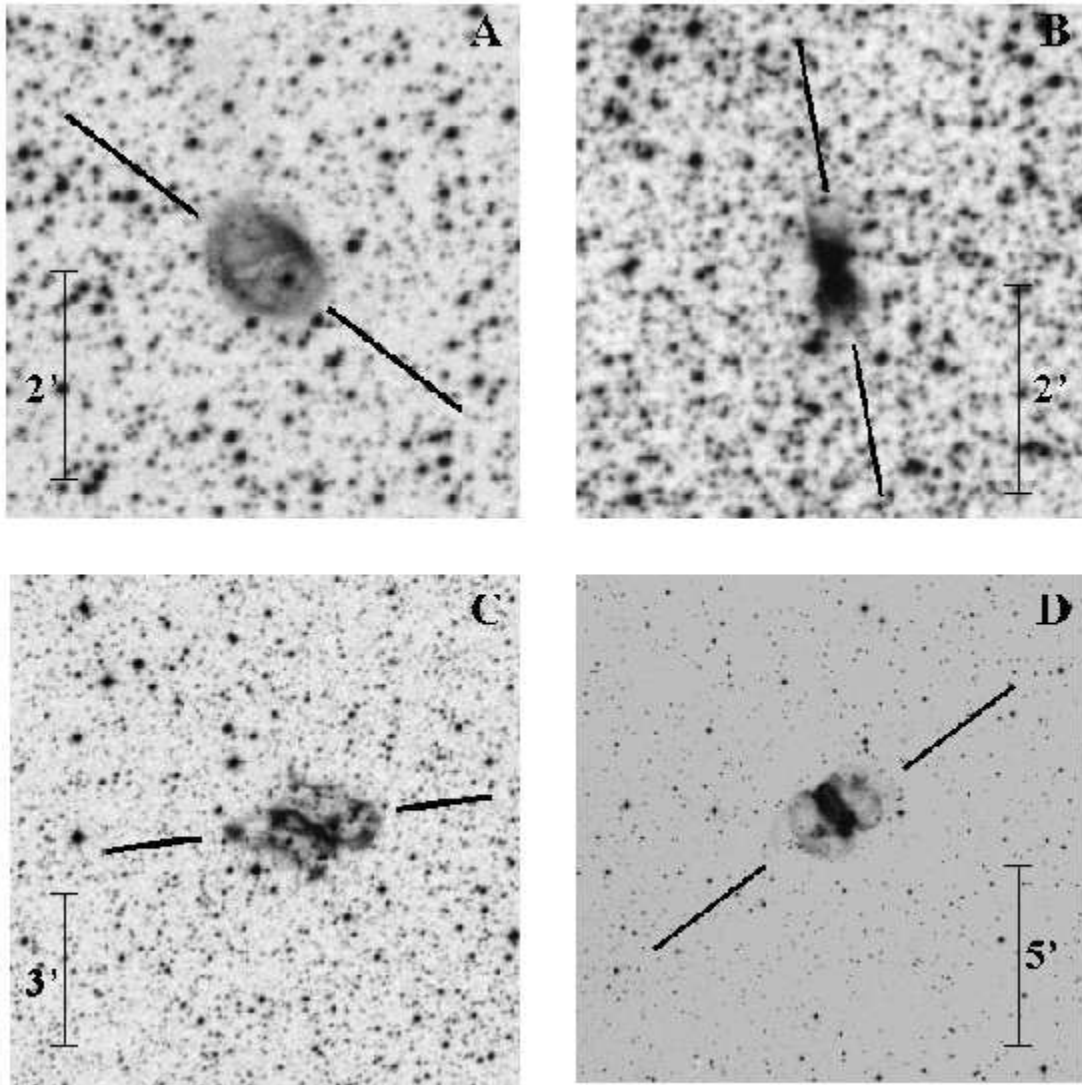


Fig. 1.— Examples of the applied measuring criteria. The objects are: A) NGC 4071, B) Mz3, C) NGC 5189 and D) NGC650. All the images belong to the DSS, red band. North is up and East to the left.

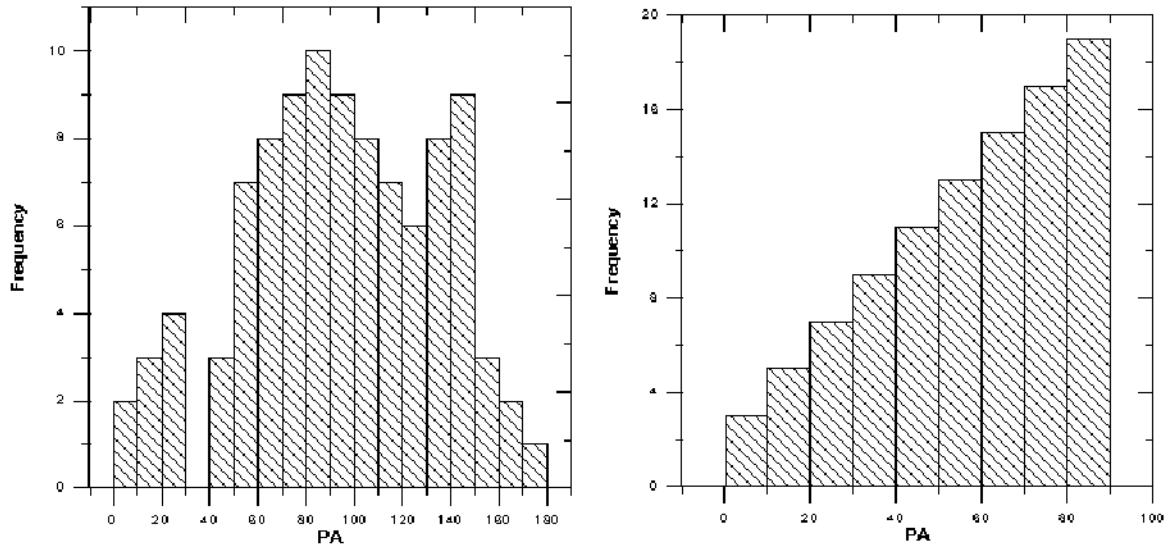


Fig. 2.— Test distribution of position angles, simulating two peaks not very near to the Galactic plane with PA computed in the interval  $[0^\circ, 180^\circ]$  (left), and the corresponding inferred distribution if the values are reported as some authors have done, in the interval  $[0^\circ, 90^\circ]$  (right).

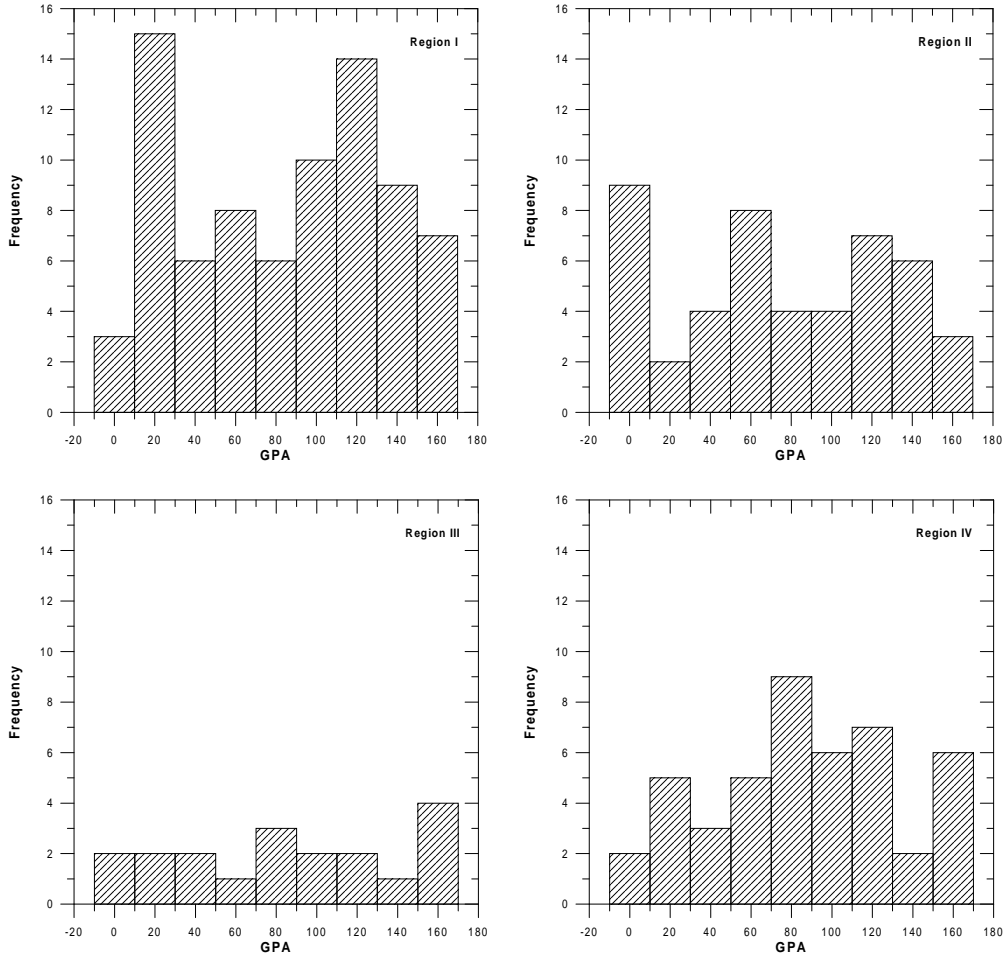


Fig. 3.— Distribution of GPA of the regions presented in table 1.

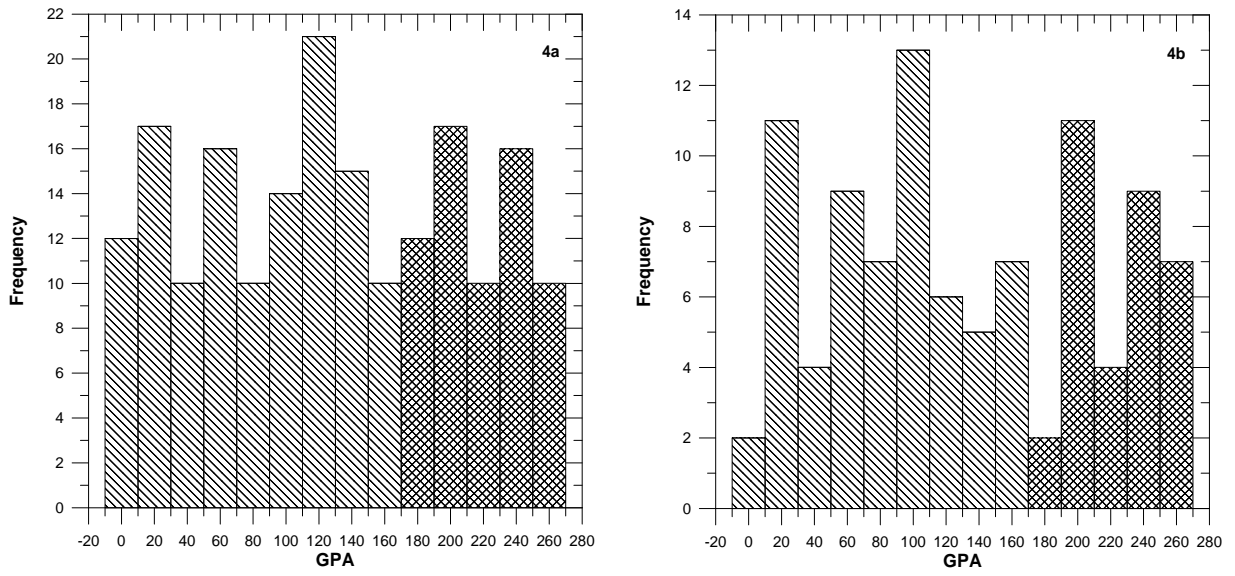


Fig. 4.— Added distribution for regions  $I + II$  (a). Inversion of the measurement of regions  $III + IV$ , considering the projection effect over the observer (b). Note that both distributions show a major peak around 100-120 degrees.

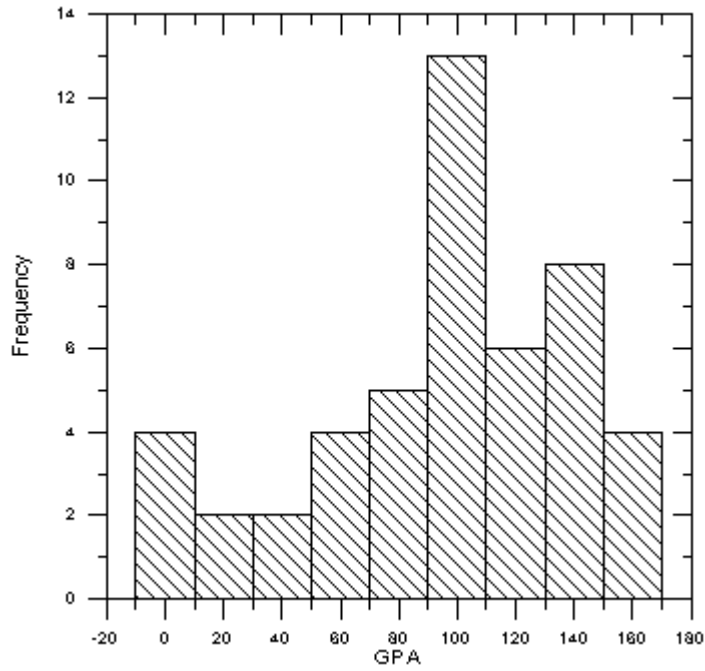


Fig. 5.— Distribution of GPA of those objects from the sample of CAM98 that have coordinates in our region I. Note the peak over  $2\sigma$  located at  $GPA \simeq 100^\circ$ .

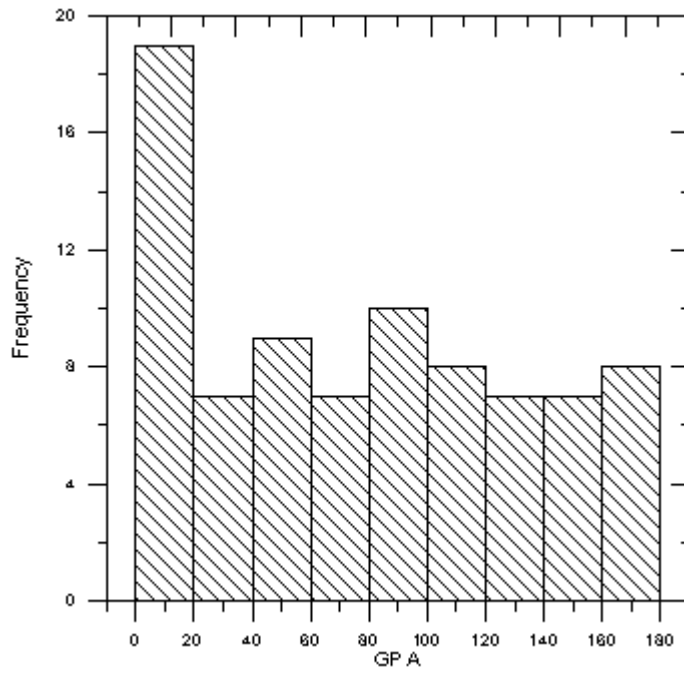


Fig. 6.— Artificial distribution of GPA, with a clear signal in the first bin.

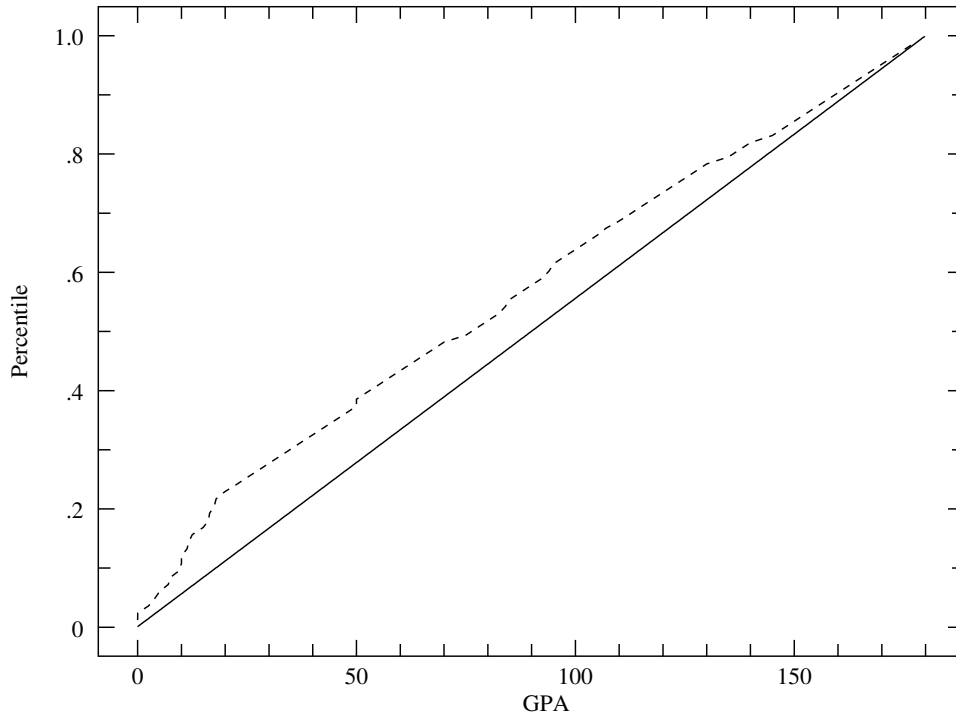


Fig. 7.— K-P test comparison percentile plot of the distribution shown in (Fig. 6). Despite the clear signal presented, the largest  $D_{max}$  yields, through the K-P test, a probability of 67%